Structure and Dynamics of Reduced *Bacillus pasteurii* Cytochrome *c*: Oxidation State Dependent Properties and Implications for Electron Transfer Processes†

Ilaria Bartalesi, Ivano Bertini,* and Antonio Rosato

Centro di Risonanze Magnetiche, University of Florence, Via Luigi Sacconi 6, and Department of Chemistry, University of Florence, Via della Lastruccia 5, 50019 Sesto Fiorentino, Italy

Received August 8, 2002; Revised Manuscript Received November 25, 2002

ABSTRACT: The solution structure of reduced *Bacillus pasteurii* cytochrome *c*, which has only 71 amino acids, has been determined by NMR to an RMSD of 0.46 ± 0.08 Å for all backbone atoms and 0.79 ± 0.08 Å for all heavy atoms and refined through restrained energy minimization. The target function out of 1645 constraints is 0.52 ± 0.11 Å^2, and the penalty function is 66 ± 12 kJ mol^{-1}. The structure appears very similar to that in the oxidized state, only Trp87 and the propionates showing significant differences. The mobility was investigated through ^{15}N R_1 and R_2 relaxation rates, ^{15}N−^{1}H NOE, and ^{1}H/^{2}H exchange. It is found that the oxidized form is generally more mobile than the reduced one. By comparing the redox-state dependence of the structural/dynamic properties of Fe-S proteins, cytochrome *c*, and blue copper proteins, hints are provided for a better comprehension of the electron transfer processes.

Electron transfer (ET)[1] processes are at the heart of a number of key physiological processes, such as aerobic and anaerobic respiration, and fatty acid metabolism. ET processes often involve one or more soluble proteins, whose sole biological function is that of shuttling the electron(s) from one redox center to another and which are normally referred to as ET proteins. There are three deeply investigated classes of such proteins, namely, cytochromes, ferredoxins, and cupredoxins (also known as blue copper proteins) (*1*). The three systems exploit respectively an iron ion in a heme cofactor, iron−sulfur cluster(s), and a copper ion to store the electron which is being shuttled. For at least one representative of each of the above three classes, the dependence of its structural and dynamic properties on the oxidation state of the metal cofactor has been characterized at atomic detail (*2*−*10*).

It is becoming increasingly apparent that a generalization of redox-dependent properties in ET proteins is not possible. Not unexpectedly, different classes of ET proteins show variations in their structural and dynamic features upon change of oxidation state, which can be profoundly diverse both in extent and in nature. Generally, redox-dependent structural variations appear to be limited and often largely restricted to side chain reorientation. On the other hand, variations in backbone dynamics as probed by either ^{15}N NMR relaxation data (which investigates motions in time scales between 10^{-12} and 10^{-9} s and/or between 10^{-5} and 10^{-3} s) or ^{1}H/^{2}H amide exchange (which investigates motions on time scales longer than 1 s) are commonly (but not always) observed. No obvious correlation between redox-dependent variations of the dynamic properties of an ET protein on the various time scales has been reported.

It is known that mitochondrial cytochromes *c* undergo some structural rearrangements upon electron transfer (*11*−*13*). The oxidized species are also more mobile than the reduced ones, particularly in the millisecond time scale (*8*) and on the time scale of ^{1}H/^{2}H exchange (*14*). It would be tempting to believe that these features are relevant for molecular recognition in the electron transfer process. Something similar holds for cytochrome b_5 (*5*, *15*). Also in Fe_2S_2 ferredoxins, it is observed that the oxidized protein is more flexible than the reduced form (*6*, *16*). On the other hand, in blue copper proteins no protein rearrangement is observed upon electron transfer nor change in mobility on any time scale (*9*). Also, in high-potential iron−sulfur proteins (HiPIP's) no protein rearrangement was observed within the NMR structural resolution (*2*, *17*). It should be noted that NMR chemical shift variations have been observed in HiPIP's and Fe_2S_2 ferredoxins as well as in cytochromes *c* and b_5, particularly for ^{15}N nuclei, upon change in the oxidation state, which are not related to any classical understanding of contact or dipolar coupling between the unpaired electron and the resonating nucleus (*3*, *9*, *18*−*20*). It is still unclear whether these chemical shift variations are caused by very subtle conformational changes or by electronic factors.

In the present work, the dependence on the oxidation state of the structural and dynamic properties of *Bacillus pasteurii* cytochrome *c* (*Bp*cyt*c* hereafter) is investigated. The solution structure and dynamics of reduced *Bp*cyt*c* are here characterized by heteronuclear NMR spectroscopy and compared to the oxidized species. The primary sequence of *Bp*cyt*c* is only

† Financial support by MIUR COFIN 2001 is gratefully acknowledged.

* Address correspondence to this author at the Centro di Risonanze Magnetiche, University of Florence, Via Luigi Sacconi 6, 50019 Sesto Fiorentino, Italy. Tel: +39 055 4574272. Fax: +39 055 4574271. E-mail: bertini@cerm.unifi.it.

[1] Abbreviations: ET, electron transfer; NMR, nuclear magnetic resonance; NOESY, nuclear Overhauser effect spectroscopy; TOCSY, total correlation spectroscopy; HSQC, heteronuclear single-quantum correlation spectroscopy; CPMG, Carr−Purcell−Meiboom−Gill; REM, restrained energy minimization; *Bp*cyt*c*, oxidized *Bacillus pasteurii* cytochrome c_{553}; RMSD, root-mean-square deviation.

10.1021/bi0266028 CCC: $25.00
Published on Web 01/01/2003

71 amino acid long, making it one of the monoheme cytochromes *c* with the highest ratio of heme to number of amino acids ever reported (*21*). Notwithstanding the relatively high charge of the polypeptide chain (−6), the small protein size is expected to result in an enhanced role of the metal ion charge due to the reduced distance of the metal site from any region of the protein backbone. This should make any effect due to ET quite evident. The putative functional role of *Bp*cyt*c* (*22*) is analogous to that of mitochondrial cytochromes *c* and to that of *Paracoccus denitrificans* cytochrome c_{552}, for which an analogous study has been reported (*23*). The comparison of the redox-dependent variations occurring in these systems is thus expected to be particularly useful in highlighting structural and dyanamic features of possible mechanistic relevance to ET processes.

MATERIALS AND METHODS

Sample Preparation. Samples of recombinant *Bp*cyt*c* were prepared as previously described (*24*). The protein was reduced by adding excess sodium dithionite, under anaerobic conditions. All samples were in 100 mM phosphate buffer, pH 7.

NMR Spectroscopy and Solution Structure Calculations. NMR spectra were acquired on reduced *Bp*cyt*c* on Bruker Avance 800, 500, and 400 spectrometers at 296 K. Data acquisition and processing were performed by using a standard Bruker software package (XWINNMR). 2D TOCSY (*25*) and 2D NOESY (*26*) spectra were acquired at 400 and 800 MHz, respectively, at two temperatures (296 and 286 K). A 3D ^{15}N-HSQC NOESY spectrum (*27*), a HNHA spectrum (*28*), and a HNHB spectrum (*29*) were acquired at 500 MHz, with a triple resonance cryoprobe. The HNHA spectrum (*28*) was used to determine $^3J_{HNH\alpha}$ coupling constants, from which constraints for the ϕ torsion angle were extracted by means of the appropriate Karplus curve (*28*).

The assignment of the ^{1}H and ^{15}N NMR signals of reduced *Bp*cyt*c* was achieved using standard procedures (*30*) through the analysis of 2D and 3D homo- and heteronuclear spectra. The 2D and 3D NOESY spectra acquired at 296 K were used to obtain upper distance limits for structure calculations. Intensities of dipolar connectivities were converted into upper distance limits through the program CALIBA, using the standard procedure (*31*). Stereospecific assignments of diastereotopic pairs were obtained using the program GLOMSA (*31*), as well as from relative cross-peak intensities in the HNHB spectrum (*29*). The ratio between intraresidue and sequential HN−Hα NOESY cross-peak intensities was used to extract constraints for the ϕ and ψ torsion angles (*32*).

All of the above constraints were used as input for the program DYANA (*33*). The heme special residue was introduced in calculations as previously described (*34*, *35*). A total of 130 random structures were generated and annealed using the standard DYANA protocol in 10000 steps. The 30 structures with lowest target function values were selected as the final DYANA family and subjected to a restrained energy minimization (REM) refinement with the program AMBER (*36*). The energy-minimized structures constituted the final REM family. The average structure of this family was built by superimposing the backbone atoms of all residues and again subjected to REM.

Structure analyses were performed with the programs PROCHECK (*37*), PROCHECK-NMR (*38*), and AQUA (*38*). Structure visualization was done with the program MOLMOL (*39*).

NMR Mobility Data Acquisition and Analysis. The NMR experiments for determination of ^{15}N longitudinal and traversal relaxation rates and ^{1}H−^{15}N NOE were recorded at 296 K at 500 MHz. R_1 and R_2 relaxation rates were obtained by fitting the cross-peak volumes (*I*), measured as a function of the relaxation delay, to a single exponential decay by using the Levenberg−Marquardt algorithm (*40*), as described in the literature (*41*). Uncertainties had been evaluated by using a Monte Carlo approach (*41*). Heteronuclear NOE values were calculated as the ratio of peak volumes in spectra recorded with and without saturation. ^{15}N relaxation data were analyzed in terms of the model-free formalism (*42*) with the Modelfree program, version 4.0, following the reported protocol (*41*), and using an isotropic model for diffusion. The amide proton−nitrogen backbone distance was taken to be 1.02 Å, and the CSA was taken to be $\delta = -172$ ppm (*43*). For the tryptophan side chain HN moiety, the CSA was taken to be $\delta = 89.0$ ppm (*44*, *45*), and for the histidine side chain HN moiety, the CSA was taken to be $\delta = -154.5$ ppm (*44*, *45*). Model selection for the model-free calculations was performed according to the procedure previously described (*41*). In the last stage of calculations τ_m was optimized together with all other parameters.

^{1}H/^{2}H exchange measurements were carried out using the same approach followed for the oxidized protein (*24*) and were fit to a monoexponential decay.

RESULTS

Solution Structure of Reduced Bpcytc. Essentially all expected resonances for ^{1}H and ^{15}N nuclei were assigned. In particular, 100% of the backbone ^{1}H and ^{15}N (except Pro residues) resonances were assigned, including the HN moiety of Ser34, which could not be detected in the oxidized protein (*24*). It was also possible to assign the resonance of the Nδ1 nucleus of the imidazole ring of the axially bound His36. The assignment achieved in this study, together with the stereospecific assignment, is reported in Table S1 of Supporting Information and has been deposited with the BMRB (entry 5597). Figure S1 shows a ^{1}H−^{15}N spectrum of the protein, labeled with the assignment.

Table 1 reports the details of the experimental constraints used for structure calculation. In total, 1541 meaningful upper distance limits (out of 1958) could be obtained from the 2D NOESY spectrum (Table 1). Figure 1A reports the distribution of the NOE constraints on a per residue basis. In addition, 104 dihedral angle constraints were employed (Table 1). All of the constraints used for solution structure calculations are listed in the Supporting Information.

The average target function of the 30 conformers constituting the DYANA family is 0.52 ± 0.08 Å^2. Their global root-mean-square deviation (RMSD) from the mean structure is 0.46 ± 0.08 Å over the entire protein backbone. The penalty function of the REM family is 66 ± 12 kJ mol^{-1} (corresponding to 0.49 ± 0.09 Å^2), while the backbone RMSD to the mean structure is 0.46 ± 0.08 Å. The RMSD for all heavy atoms is 0.78 ± 0.09 Å. The RMSD values for

Table 1: Summary of NMR Constraints Used for Structure Calculation, Restraint Violations, Structural Statistics, and Energetics for the Restrained Energy-Minimized Solution Structure of Reduced Cytochrome *c* from *B. pasteurii*

		REM		⟨REM⟩	
	no.	av no. of violations per conformer	RMS violation per restraint	no. of violations	RMS violation per restraint
structural constraint					
meaningful NOESY (total NOESY)	1541 (1958)	27.0 ± 2.60	0.017 ± 0.002	35	0.023
intraresidue	207	1.47 ± 0.67	0.008 ± 0.004	1	0.0040
sequential	341	7.37 ± 1.70	0.022 ± 0.004	10	0.025
medium range	458	6.70 ± 1.81	0.013 ± 0.002	10	0.016
long range	535	11.5 ± 2.04	0.017 ± 0.002	14	0.029
ϕ	52	0.17 ± 0.45	0.08 ± 0.20	1	1.564
ψ	52	1.63 ± 0.95	0.71 ± 0.41	2	2.383
violations between 0.1 and 0.3 Å		10.0 ± 2.6			17
violations larger than 0.3 Å		0.35 ± 0.48			2
largest distance violation (Å)		0.39		0.35	
largest ϕ violation (deg)		8.6		11.3	
largest ψ violation (deg)		13.5		15.1	
energetics					
total target function		0.52 ± 0.11		1.0	
Amber average energy (kJ/mol)		−3330 ± 150		−3319	
structure analysis					
completeness of ^{15}N backbone assignment	100%				
completeness of ^{1}H backbone assignment	100%				
structural constraints per residue	23.2				
residues in most favored regions[a] (%)		85.8		88.0	
residues in allowed regions[a] (%)		13.9		12.0	
residues in generously allowed regions[a] (%)		0.2		0.0	
residues in disallowed regions[a] (%)		0.0		0.0	
overall *G*-factor[b]		−0.51		−0.17	

[a] As defined by the Ramachandran plot. [b] As defined in the program PROCHECK (*37*).

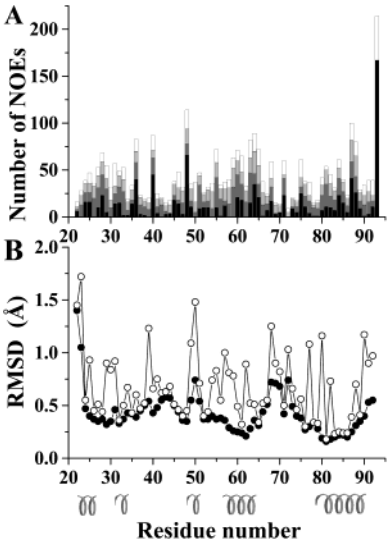

FIGURE 1: (A) Number of NOEs per residue for reduced *B. pasteurii* cytochrome *c*. White, light gray, dark gray, and black bars indicate intraresidue, sequential, and medium-range, or long-range connectivities, respectively. The NOE constraints for the heme moiety are reported as belonging to residue 93. (B) Per residue plot of backbone (filled squares) and heavy atoms (open circles) RMSD with respect to the mean structure for the final family of conformers. The position of α-helices is depicted at the bottom of the picture.

the REM family are plotted on a per residue basis in Figure 1B. An overview of the quality parameters for the REM family, as well as for the restrained energy-minimized mean structure, is given in Table 1. They indicate that the obtained structure has a very good quality. Coordinates for the final family of conformers and for the energy-minimized average structure have been deposited in the PDB (PDB entry 1N9C).

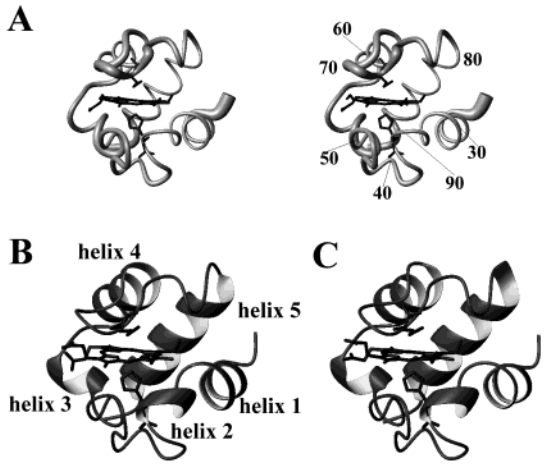

FIGURE 2: (A) Stereoview (side by side) of the backbone of the final family of conformers of reduced *B. pasteurii* cytochrome *c* represented as a tube with variable radius, proportional to the backbone RMSD of each residue. Comparison ribbon display of the energy-minimized average structure of (B) reduced and (C) oxidized *B. pasteurii* cytochrome *c*. This figure was prepared with the program MOLMOL (*39*).

A "sausage" view of the backbone is shown in Figure 2, which also depicts the secondary structure elements resulting from calculations. The protein displays an all-helical fold, as is commonly found for *c*-type cytochromes (*46*), with two long helices at the N- and C-termini (α_1 and α_5, spanning residues 24−30 and 80−91, respectively), and three additional helices: two short helices involving residues 32−34 (α_2) and 51−54 (α_3) and a longer helix in position 57−66 (α_4). The first ligand to the iron ion is His36, and the second ligand is Met71; both are located in two external loops.

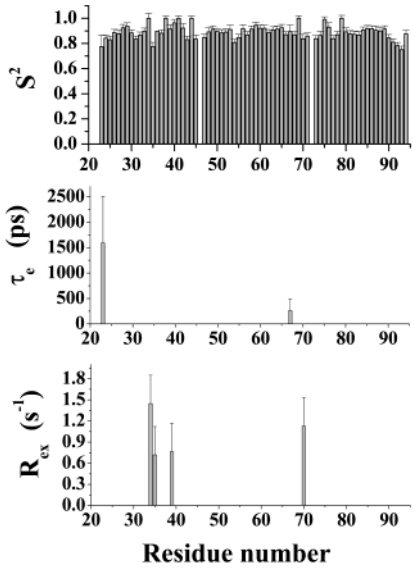

FIGURE 3: Per residue plots of the best-fit model-free parameters obtained from ^{15}N relaxation data for reduced cytochrome *c* from *B. pasteurii*. Residues 93 and 94 represent respectively the side chain NH moieties of Trp87 and His36.

Protein Mobility from ^{15}N Relaxation and Amide Exchange Data. ^{15}N relaxation data to be used in the model-free analysis were obtained for all non-proline residues (excluding also the N-terminal residue Val22), for the Nϵ1 of Trp87, and for the Nδ1 of His36. The average R_1 and R_2 and heteronuclear NOE were respectively 2.59 $\pm$ 0.13, 7.05 $\pm$ 0.30, and 0.76 $\pm$ 0.05 at 500 MHz. For all residues three data were used as imput for the Modelfree program, namely, R_1, R_2, and NOE at 500 MHz.

The results of the model-free fittings are shown in Figure 3. The data for all residues could be fitted with a maximum of two adjustable parameters, the large majority of residues being adequately fitted by the simplest model of the Modelfree program (*41*, *47*). Only two residues were fitted thus using τ_e as an adjustable parameter: Asp23, which is the second residue of the sequence, and Gly67 (Figure 3). Inclusion of R_{ex} (up to 1.45 s^{-1}) in the fittings was required for residues Ser34, Cys35, Asp39, and Gly70 (Figure 3). The average S^2 value over the backbone NH moieties of all residues was 0.89 $\pm$ 0.06. The NH moieties of the side chains of His36 and Trp87 could both be fitted using only S^2 as an adjustable parameter. The resulting S^2 values were 0.88 and 0.75, respectively (Figure 3). The best-fit parameters obtained from model-free calculations are listed in the Supporting Information.

DISCUSSION

Comparison of the Solution Structure of Bpcytc in the Oxidized and Reduced State. Figure 2 shows a comparison of the solution structures of oxidized and reduced *Bp*cyt*c*. It can be seen that the two structures are very similar, with an RMSD between all backbone atoms of only 0.34 Å. The largest differences between the conformation of the protein backbone in the two forms lie in the loop regions connecting the various helices. These regions most often coincide with relative maxima of the RMSD per residue, and thus the differences observed are marginally significant. The backbone conformation in the two solution structures is also very similar to that observed in the crystal structure of the oxidized protein, which was solved at pH 4.6 in the oxidized state (*48*).

As far as the conformation of side chains is concerned, the most relevant redox-state-dependent variation is that of the position of Trp87, whose side chain in the reduced form moves toward the interior of the protein with respect to that observed in the oxidized structure. The motion preserves the orientation of the plane of the Trp87 side chain and can be described as a rotation centered on its Cα atom around an axis normal to the plane of the side chain, whose atoms are displaced up to 1.4 Å. This change in position is substantiated by NOEs between the side chain of Trp87 and the backbone amide moiety of Val28, which are observed in reduced *Bp*cyt*c* and are not compatible with the position of the side chain observed for the oxidized protein. This movement brings the side chain of Tp87 closer to the heme cofactor by slightly more than 1 Å. It is possible that this structural change may contribute to tuning the heme redox potential [which in the present protein is quite low with respect to mitochondrial cytochromes, being only +47 mV (*49*)]. Recently, the existence of a redox-state-dependent gating mechanism has been proposed for rubredoxin, a small ET protein using an iron ion as cofactor (*50*). Whether such effects are also affecting the ET rate depends on the kinetics of the structural rearrangement, on which the present data do not provide information. It is worthwhile recalling that the redox potentials of ET partners can vary upon complexation with the partner. This has been proposed for mitochondrial cytochrome *c* (*51*), as well as for other systems, such as cytochrome b_5 (*52*). However, complex formation in these systems is driven by electrostatic recognition between the partners; in the present system, structure modeling studies instead suggest that hydrophobic interactions may guide the interaction with the partner (*24*).

Other differences in side chain conformation are restricted to highly solvent-exposed residues, e.g., Glu25. The interpretation of these differences is difficult, as they may be also linked to slight variations in pH and/or ionic strength (e.g., due to the addition of reductant) between the oxidized and reduced protein samples. There are no buried titratable side chains in *Bp*cyt*c* besides the δNH moiety of the imidazole ring of the iron-bound His36. The variation of the charge of the iron ion is likely to induce a decrease of the acidity (i.e., K_a) of this group upon reduction. The available data, however, clearly show that this group is protonated at neutral pH in both oxidized and reduced *Bp*cyt*c*. It is also to be noted that this group forms a redox-state-independent hydrogen bond with Pro46 (see later), which prevents its deprotonation. As far as solvent-exposed side titratable side chains are concerned, large variations of their pK_a's appear unlikely due to the fact that they protrude in the solvent and should thus be shielded from charge variations at the iron site by the high dielectric constant of bulk water.

A number of researchers have highlighted that in electron transfer hemoproteins a change in the oxidation state of the iron ion is often linked to a structural rearrangement of the heme substituents (*46*, *53*, *54*). In the present case, both heme propionates protrude in solution in both oxidation states. A conformational change is nevertheless observed for propionate 7, caused by a 20−30° rotation around the bond between its α and β carbons and by a rotation of the terminal

carboxylate group. This rotation brings the carboxylate in a position allowing the formation of a new hydrogen bond with the side chain of Gln66, which also experiences a small structural rearrangement. Propionate 6, whose conformation is less well defined than for propionate 7, instead is found to experience a structural rearrangement causing it to form hydrogen bonds with the backbone amide of Gly70 in several conformers of reduced *Bp*cyt*c*.

It is well-known that in essentially all *c*-type cytochromes the side chain of the axial His (His36 in the present system) is hydrogen-bonded to the carbonyl oxygen of a nearby conserved Pro (here Pro46) through its exchangeable Hδ1 proton (*24*, *55*, *56*). In the present system, the cross-peak due to the NH moiety of the imidazole could be observed in ^{1}H$-^{15}$N HSQC experiments, and this moiety could thus be directly investigated. Its relatively high S^2 value (0.88) and the slow rate of exchange in D_2O of the Hδ1 proton provide direct experimental indications that the mentioned H-bond is present in solution.

Comparison of the Mobility of Bpcytc in the Oxidized and Reduced State. The average S^2 for the backbone amide moieties in reduced *Bp*cyt*c* is 0.89 $\pm$ 0.06, which compares with 0.86 $\pm$ 0.05 for the oxidized protein (*24*). This difference corresponds to a generalized slight increase (on average ca. 0.03) of S^2 along the protein chain in the reduced with respect to the oxidized form, which however is lower than the sum of the average errors on S^2 in the two oxidation states, which is around 0.05. The most notable exception is constituted by residues 35$-$37, which are slightly more flexible in the reduced state (up to a 0.1 decrease in S^2). Notably this corresponded to the most rigid region in the oxidized protein (*24*). Also the per residue profile of the S^2 values shown in Figure 3 very closely resembles that of the oxidized protein, with enhanced flexibility at the N- and C-terminal termini and relatively more rigid stretches around the iron axial ligands. Globally, the backbone of the protein appears to be rigid on the nanosecond to picosecond time scale in both oxidation states. The NH moiety of the side chain of Trp87 is slightly more mobile in the reduced than in the oxidized form ($S^2 = 0.75$ and 0.83, respectively), even though it is less solvent-exposed in the former system.

The most prominent dynamic feature of oxidized *Bp*cyt*c* was the presence of quite important conformational exchange processes involving residues 33, 39$-$41, and 44, while the backbone amide moiety of residue 34 could not be detected in NMR spectra (*24*). These processes are still observable for residues 34 and 35 in the reduced state, albeit with small R_{ex} values (lower than 1 s^{-1}, to be compared with values between 2 and 7 s^{-1} for the oxidized protein), which presumably indicates that the distribution of conformers in equilibrium in the reduced state is largely biased toward one dominant species (Figure 3). It is to be mentioned that in principle pseudocontact shifts due to the paramagnetism of the oxidized species could make the observed R_{ex} values for the oxidized species larger than what would be measured in an otherwise identical diamagnetic sample. However, it has been demonstrated in the similar case of cytochrome b_5 that this in practice is not a problem (*5*). Additionally, in the reduced species an exchange process could be observed for Gly70 (Figure 3), which is not observed in oxidized *Bp*cyt*c*.

The kinetics of exchange of amide protons in D_2O has been determined for both oxidation states and globally is significantly faster in the oxidized form, as also observed for other *c*-type cytochromes (*13*, *14*, *23*). The ratio of the apparent exchange rates [k_{exch} (*57*)] determined in the two oxidation states is shown on a per residue basis in Figure 4. It can be seen that generally for residues in the exchange regime amenable to NMR characterization the exchange rates in the oxidized protein are 1$-$2 orders of magnitude larger than in the reduced state. The larger variations in the residue-specific opening constants appear to cluster in helices α4 and α5. These two helices are parallel and in reciprocal contact, suggesting that there may be a concerted mechanism by which the protection of the amide groups in this region of the protein is enhanced in reduced *Bp*cyt*c*.

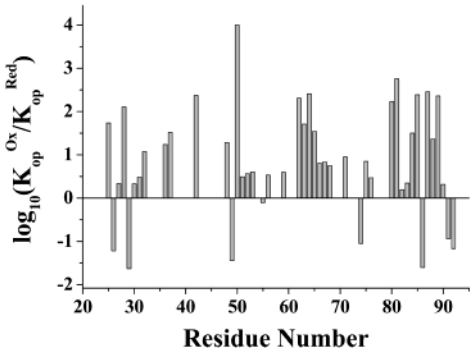

FIGURE 4: Comparison of the per residue exchange rates (k_{exch}) observed in the oxidized and reduced forms of cytochrome *c* from *B. pasteurii*.

The data discussed in this and the preceding section provide a thorough picture of the influence of the oxidation state of the heme iron on the structural and dynamic properties of *Bp*cyt*c*. To fully understand the role played by the heme cofactor, further insights can be obtained from the investigation of the apo form of the protein, which will be tackled in our laboratory.

Implications for Electron Transfer Proteins. The results of the comparison between the structural and dynamic properties of oxidized and reduced *Bp*cyt*c* can be summarized as follows: (i) there are no gross conformational rearrangements upon reduction; (ii) relatively small structural changes are observed for some side chains and, most notably, for the side chain of Trp87 and for the heme propionates; (iii) the reduced form of *Bp*cyt*c* is less flexible than the oxidized on time scales longer than 10 μs, while both states are rigid on the subnanosecond time scale. The occurrence of a conformational rearrangement of one heme propionate upon change of oxidation state appears to be a quite general feature of cytochromes, not only of *c*-type (*13*, *34*, *58*$-$*60*), although it has not been observed for *P. denitrificans* cytochrome c_{552} (*23*). This rearrangement is most likely caused by the variation of the electrostatics induced by the change in charge at the iron ion. ET studies suggest that it may be of relevance for the ET process mediated by cytochrome *c* (*13*, *23*, *60*$-$*62*). The redox-state-dependent dynamic behavior of *Bp*cyt*c* (see point iii above) is analogous to that of mitochondrial and *P. denitrificans c*-type cytochromes (*13*, *23*, *34*, *60*), and opposite to that, less common, of *Desulfovibrio vulgaris* cytochrome c_{553} (*4*). It is interesting to observe that the latter is a strict anaerobic organism, while the other cytochromes, as well as *Bp*cyt*c*, are involved in aerobic respiration. This suggests that there is a correlation between the features of the redox-state-dependent dynamic

behavior of *c*-type cytochromes and the biochemical pathway they belong to.

Of the three best characterized classes of ET proteins, namely, cytochromes, ferredoxins, and blue copper proteins, the former two display a distinct dependence of their dynamic properties on the redox state (*5*−*8*, *23*), while the third one does not (*9*). This difference may be related to the fact that optimal ET transfer occurs when the reorganization at the redox site is minimal. The copper site in blue copper proteins may thus require a more rigid protein structure enforcing minimal reorganization than is the case for cytochromes and ferredoxins. On the other hand, it is tempting to link the common behavior of cytochromes and ferredoxins to a functional mechanism in which the recognition by physiological partners as a function of redox state is fine-tuned through differential sampling of the available conformational space by the oxidized and reduced forms of the protein. In *Bp*cyt*c*, the oxidized species samples a larger conformational space with respect to the reduced one (see, for instance, Figure 4). Thus, selectivity for binding to oxidized *Bp*cyt*c* with respect to the reduced species would be enhanced if the partner were preorganized to better bind a conformer relatively distant from the essentially redox-state-independent average structure. On the other hand, a partner designed to optimally recognize the average protein structure would have greater affinity for the reduced vs the oxidized species. Available data for putidaredoxin, an Fe_2S_2 ferredoxin, are in keeping with this hypothesis (*3*, *6*). It is to be noted that a certain degree of selectivity between oxidized and reduced cytochrome *c* is desirable, as it reduces inhibition in the ET process. Interestingly, in the more evolved mitochrondrial cytochrome *c*, the variation in the protein dynamic properties upon change of oxidation state occurs to a larger extent than in the case of the present bacterial cytochrome and involves also regions which have been shown to be directly at the interface for partner recognition (*7*, *8*). It is tempting to speculate that the selection mechanism depicted above may have been enhanced along evolution, through the design of a more elaborate loop structure, and also at the expense of the stability of the heme environment (*63*).

ACKNOWLEDGMENT

We thank Dr. L. Thony Meyer for providing us with *pEC*86 and Dr. S. Ciurli for encouraging us to pursue this research.

SUPPORTING INFORMATION AVAILABLE

Four tables listing respectively ^{15}N and ^{1}H NMR chemical shifts in reduced *Bp*cyt*c*, upper distance limits and dihedral angle constraints used in solution structure calculations, and best-fit model-free parameters and one figure showing the $^{1}H-^{15}N$ HSQC spectrum of reduced *Bp*cyt*c*. This material is available free of charge via the Internet at http://pubs.acs.org.

REFERENCES

1. Bertini, I., Sigel, A., and Sigel, H. (2001) in *Handbook on Metalloproteins*, Marcel Dekker, New York.
2. Bertini, I., Eltis, L. D., Felli, I. C., Kastrau, D. H. W., Luchinat, C., and Piccioli, M. (1995) *Chem. Eur. J. 1*, 598−607.
3. Pochapsky, T. C., Kostic, M., Jain, N., and Pejchal, R. (2001) *Biochemistry 40*, 5602−5614.
4. Blanchard, L., Blackledge, M. J., Marion, D., and Guerlesquin, F. (1996) *FEBS Lett. 3889*, 203−209.
5. Banci, L., Bertini, I., Cavazza, C., Felli, I. C., and Koulougliotis, D. (1998) *Biochemistry 37*, 12320−12330.
6. Sari, N., Holden, M. J., Mayhew, M. P., Vilker, V. L., and Coxon, B. (1999) *Biochemistry 38*, 9862−9871.
7. Fetrow, J. S., and Baxter, S. M. (1999) *Biochemistry 38*, 4480−4492.
8. Barker, P. B., Bertini, I., Del Conte, R., Ferguson, S. J., Hajieva, P., Tomlinson, E. J., Turano, P., and Viezzoli, M. S. (2001) *Eur. J. Biochem. 268*, 4468−4476.
9. Bertini, I., Bryant, D. A., Ciurli, S., Dikiy, A., Fernández, C. O., Luchinat, C., Safarov, N., Vila, A. J., and Zhao, J. (2001) *J. Biol. Chem. 276*, 47217−47226.
10. Assfalg, M., Banci, L., Bertini, I., Ciofi-Baffoni, S., and Barker, P. D. (2001) *Biochemistry 40*, 12761−12771.
11. Gao, Y., Boyd, J., Pielak, G. J., and Williams, R. J. P. (1991) *Biochemistry 30*, 1928−1934.
12. Berghuis, A. M., and Brayer, G. D. (1992) *J. Mol. Biol. 223*, 959−976.
13. Banci, L., Bertini, I., Bren, K. L., Gray, H. B., Sompornpisut, P., and Turano, P. (1997) *Biochemistry 36*, 8992−9001.
14. Baxter, S. M., and Fetrow, J. S. (1999) *Biochemistry 38*, 4493−4503.
15. Dangi, B., Blankman, J., Miller, C. J., Volkman, B. F., and Guiles, R. D. (1998) *J. Phys. Chem. B 102*, 8201−8208.
16. Lyons, T. A., Ratnaswamy, G., and Pochapsky, T. C. (1996) *Protein Sci. 5*, 627−639.
17. Bertini, I., Dikiy, A., Kastrau, D. H. W., Luchinat, C., and Sompornpisut, P. (1995) *Biochemistry 34*, 9851−9858.
18. Bertini, I., Luchinat, C., and Turano, P. (2000) *JBIC, J. Biol. Inorg. Chem. 5*, 761−764.
19. Boyd, J., Dobson, C. M., Morar, A. S., Williams, R. J. P., and Pielak, G. J. (1999) *J. Am. Chem. Soc. 121*, 9247−9248.
20. Lehmann, T. E., Luchinat, C., and Piccioli, M. (2002) *Inorg. Chem. 41*, 1679−1683.
21. Barker, P. D., and Ferguson, S. J. (1999) *Struct. Folding Des. 7*, R281−R290.
22. Vanderberghe, I. H., Ciurli, S., Benini, S., and Van Beeumen, J. (1999) *Biochem. Biophys. Res. Commun. 264*, 380−387.
23. Reincke, B., Perez, C., Pristovsek, P., Lucke, C., Ludwig, C., Lohr, F., Ludwig, B., and Ruterjans, H. H. (2001) *Biochemistry 40*, 12312−12320.
24. Banci, L., Bertini, I., Ciurli, S., Dikiy, A., Dittmer, J., Rosato, A., Sciara, G., and Thompsett, A. (2002) *ChemBioChem 3*, 299−310.
25. Bax, A., and Davis, D. G. (1985) *J. Magn. Reson. 63*, 207−213.
26. Wider, G., Macura, S., Kumar, A., Ernst, R. R., and Wüthrich, K. (1984) *J. Magn. Reson. 56*, 207−234.
27. Wider, G., Neri, D., Otting, G., and Wüthrich, K. (1989) *J. Magn. Reson. 85*, 426−431.
28. Vuister, G. W., and Bax, A. (1993) *J. Am. Chem. Soc. 115*, 7772−7777.
29. Archer, S. J., Ikura, M., Torchia, D. A., and Bax, A. (1991) *J. Magn. Reson. 95*, 636−641.
30. Wüthrich, K. (1986) in *NMR of Proteins and Nucleic Acids*, Wiley, New York.
31. Güntert, P., Braun, W., and Wüthrich, K. (1991) *J. Mol. Biol. 217*, 517−530.
32. Gagne′, R. R., Tsuda, S., Li, M. X., Chandra, M., Smillie, L. B., and Sykes, B. D. (1994) *Protein Sci. 3*, 1961−1974.
33. Güntert, P., Mumenthaler, C., and Wüthrich, K. (1997) *J. Mol. Biol. 273*, 283−298.
34. Banci, L., Bertini, I., Gray, H. B., Luchinat, C., Reddig, T., Rosato, A., and Turano, P. (1997) *Biochemistry 36*, 9867−9877.
35. Banci, L., Bertini, I., Cremonini, M. A., Gori Savellini, G., Luchinat, C., Wüthrich, K., and Güntert, P. (1998) *J. Biomol. NMR 12*, 553−557.
36. Case, D. A., Pearlman, D. A., Caldwell, J. W., Cheatham, T. E., Ross, W. S., Simmerling, C. L., Darden, T. A., Merz, K. M., Stanton, R. V., Cheng, A. L., Vincent, J. J., Crowley, M., Tsui, V., Radmer, R. J., Duan, Y., Pitera, J., Massova, I., Seibel, G. L., Singh, U. C., Weiner, P. K., and Kollman, P. A. (1999) in *AMBER 6*, University of California, San Francisco.
37. Laskowski, R. A., MacArthur, M. W., Moss, D. S., and Thornton, J. M. (1993) *J. Appl. Crystallogr. 26*, 283−291.
38. Laskowski, R. A., Rullmann, J. A. C., MacArthur, M. W., Kaptein, R., and Thornton, J. M. (1996) *J. Biomol. NMR 8*, 477−486.

39. Koradi, R., Billeter, M., and Wüthrich, K. (1996) *J. Mol. Graphics 14*, 51−55.
40. Marquardt, D. W. (1963) *J. Soc. Ind. Appl. Math. 11*, 431−441.
41. Mandel, M. A., Akke, M., and Palmer, A. G., III (1995) *J. Mol. Biol. 246*, 144−163.
42. Lipari, G., and Szabo, A. (1982) *J. Am. Chem. Soc. 104*, 4546−4559.
43. Ishima, R., and Torchia, D. A. (2000) *Nat. Struct. Biol. 7*, 740−743.
44. Cross, T. A., and Opella, S. J. (1983) *J. Am. Chem. Soc. 105*, 306−308.
45. Ramamoorthy, A., Wu, C. H., and Opella, S. J. (1997) *J. Am. Chem. Soc. 119*, 10479−10486.
46. Scott, R. A., and Mauk, A. G. (1996) in *Cytochrome c. A multidisciplinary approach*, University Science Books, Sausalito, CA.
47. Mandel, M. A., Akke, M., and Palmer, A. G., III (1996) *Biochemistry 35*, 16009−16023.
48. Benini, S., Rypniewski, W., Wilson, K. S., Van Beeumen, J., and Ciurli, S. (2000) *Biochemistry 39*, 13115−13126.
49. Benini, S., Borsari, M., Ciurli, S., Dikiy, A., and Lamborghini, M. (1998) *J. Biol. Inorg. Chem. 3*, 371−382.
50. Min, T., Ergenekan, C. E., Eidsness, M. K., Ichiye, T., and Kang, C. (2001) *Protein Sci. 10*, 613−621.
51. Hirota, S., Endo, M., Hayamizu, K., Tsukazaki, T., Takabe, T., Kohzuma, T., and Yamauchi, O. (1999) *J. Am. Chem. Soc. 121*, 849−855.
52. Rivera, M., Seetharaman, R., Girdhar, D., Wirtz, M., Zhang, X., Wang, X., and White, S. (1998) *Biochemistry 37*, 1485−1494.
53. Mathews, F. S. (1985) *Prog. Biophys. Mol. Biol. 45*, 1−56.
54. Banci, L., Bertini, I., Luchinat, C., and Turano, P. (2000) in *The Porphyrin Handbook* (Kadish, K. M., Smith, K. M., and Guilard, R., Eds.) pp 323−350, Academic Press, San Diego, CA.
55. Banci, L., Bertini, I., Rosato, A., and Varani, G. (1999) *J. Biol. Inorg. Chem. 4*, 824−837.
56. Bartalesi, I., Bertini, I., Hajieva, P., Rosato, A., and Vasos, P. (2002) *Biochemistry 41*, 5112−5119.
57. Bai, Y., Milne, J. S., Mayne, L., and Englander, S. W. (1993) *Proteins: Struct., Funct., Genet. 17*, 75−86.
58. Arnesano, F., Banci, L., Bertini, I., and Felli, I. C. (1998) *Biochemistry 37*, 173−184.
59. Banci, L., Bertini, I., De la Rosa, M. A., Koulougliotis, D., Navarro, J. A., and Walter, O. (1998) *Biochemistry 37*, 4831−4843.
60. Banci, L., Bertini, I., Huber, J. G., Spyroulias, G. A., and Turano, P. (1999) *JBIC, J. Biol. Inorg. Chem. 4*, 21−31.
61. Casimiro, D. R., Richards, J. H., Winkler, J. R., and Gray, H. B. (1993) *J. Phys. Chem. 97*, 13073−13077.
62. Langen, R., Spielmann, H. P., Germanas, J. P., Richards, J. H., Winkler, J. R., and Gray, H. B. (1995) *Science 268*, 1733−1735.
63. Bartalesi, I., Bertini, I., Ghosh, K., Rosato, A., and Turano, P. (2002) *J. Mol. Biol. 321*, 693−701.

BI0266028